Supplemental Information

Photonic Chiplet Interconnection via 3D-Nanoprinted Interposer

Huiyu Huang[1,†], Zhitian Shi[1,†], Giuseppe Talli[2], Maxim Kuschnerov[2], Richard Penty[1], and Qixiang Cheng[1,*]

[1] Centre for Photonic Systems, Electrical Engineering Division, Department of Engineering, University of Cambridge, Cambridge CB3 0FA, U.K.

[2] Huawei Technologies Duesseldolf GmbH, European Research Center, Riesstraße 25, 80992 Munich, Duesseldolf, Gemany.

[†] These authors contributed equally to this work.

*qc223@cam.ac.uk

S1. Recent development of 3D-nanoprinted coupling methods for photonics applications

3D-nanoprinting technology has shown its strength in photonic packaging via fabricating in-situ optical couplers for mode match, especially when dealing with special cases that involve non-standardized optical fibres or waveguides. In 2016, Dietrich et al. [1] demonstrated a convex-lens-based approach which shows a very low loss of 0.5 dB/facet using the active alignment method. Later [2], the same group demonstrated a series of lens-based couplers for connecting different platforms, all aligned dynamically. Gordillo et al. [3] printed an adiabatic-taper-based coupler with a funnel structure to enable passive alignment, which shows a good coupling efficiency of 2.5 dB/facet over a broad bandwidth of 100 nm. Blaicher et al. [4] presented their optical receiver using a convex lens to couple optical beam with a tapered coupler. This design is capable of mode size matching with a large conversion ratio. Yet, it is a one-way design that makes it hard to be used as an I/O port. Gehring et al. [5] introduced a very similar solution, which additionally has a reflecting surface at the backside of the convex lens, allowing a re-confinement of the light, making it a dual-way coupler. The coupler operates at the wavelength around 700 nm and the coupling efficiency drops quickly after 800 nm, far from the commonly used optical communication bands. In the same year, an optical-communication-compatible version was reported by the authors [6]. It is a very good design for single-chip applications, while the out-of-plane angle is not ideal for chip-to-chip coupling. Yu et al. [7] tried to couple the light with an on-chip printed freeform reflector. The reflector operates at wavelengths around 800 nm at a low coupling loss of about 1 dB/facet and is aligned actively. Gordillo et al. [8] published another manuscript on 3D-printed coupler that is equipped with a funnel-like structure to achieve passive alignment and stable fiber fixing. The impressive excess loss of 0.05 dB/facet proved that the mechanical fiber fixer is helpful to realize fully passive alignment, but the intrinsic grating coupler introduces a high coupling loss of 4.7 dB/facet with limited bandwidth. Chen et al. [9] demonstrated another one-way coupler, which is for light emitter. The coupling loss is reported to be 3 dB/facet and the 1 dB-loss-bandwidth is over 100 nm. In the same year, Luo et al. [10] published another approach which resembles Blaicher's work, still as a one-way coupler. Differently, Luo's model uses a reverse-pyramid-shaped structure as the light collector.

Supplemental Information

In 2023, Yu et al. reported their improved version of the on-chip printed freeform lens array. It shows good off-plane coupling efficiency after the fiber array is actively aligned with the lenses. Xu et al. [7], [11] reported a full-lens-based multi-platform integration in 2023. These demonstrates are summarized in Table S1 with key figure of merits outlined. Table S2 summarizes notable demonstrations of cross-platform integrations with different technologies.

Table S1. Recent development of 3D-nanoprinted coupling methods for photonics applications

ref.	coupling type	emitter	receiver	loss (dB/facet)	alignment	mode size conversion ratio	broadband
[1]	lenses	SMF 10 μm	SMF 10 μm	0.5	dynamic	1:1	@ 1550 nm
[2]	lenses	SMF 10 μm	TriPleX 11 μm	2.5	dynamic	0.9:1	@ 1550 nm
[3]	direct	SMF 10 μm	polymer WG	2.5	passive	-	no change over 1520 nm -1620 nm
[4]	taper	SMF 10 μm	Si WG	0.8	dynamic	-	1 dB loss over 100 nm (expected)
[5]	taper	S630-HP 4.2 μm	SiN WG	3.1	dynamic	-	@ 700 nm
[6]	taper	SMF 10 μm	SiN WG	1.6	dynamic	-	1 dB over 1480 nm -1680 nm
[7]	EC	Polymer WG 2.3 μm	780-HP 5 μm	0.9	dynamic	0.5:1	@ 856 nm
[8]	grating coupler	SMF 10 μm	Si WG	0.05	passive	-	@ 1544 nm
[9]	direct	Polymer WG 10 μm	multi-core fibers 10 μm	3	dynamic	1:1	1 dB loss over 100 nm
[10]	taper	SMF 10 μm	SU-8 WG 3.5 μm	1.04	dynamic	3:1	1 dB loss over 100 nm
[7]	EC	SMF 10 μm	SiN WG	0.37	dynamic	-	1 dB loss over 500 nm
[11]	EC	SMF 10 μm	SiP-chip 10 μm	1.44	passive	1:1	1 dB loss over 1475 nm-1625 nm
this work	EC	SMF 10 μm	polymer WG	2.2	passive	5:2	1 dB loss over 1500 nm-1600 nm

Table S2. Noticeable heterogeneous integration approaches for photonics packaging

Ref	**Material interfacing method**	**Integration technology**	**Coupling loss (dB/facet)**	**Material platforms**	**Bandwidth**	**Alignment**
[12]	edge coupling	flip-chip bonding	1.5	InP and silicon wafer	@ 1550 nm	Active
[13]	evanescent coupling	wafer bonding	12	lithium niobates and III–V	@ 1580 nm	Lithograph
[14]	edge coupling	epitaxial growth	Not mentioned	2H-MoTe2 on arbitrary interface	@ 1300 nm	Lithograph
[15]	adiabatic coupling	micro transfer printing	12.3	III–V and silicon	@ 1558 nm	Passive
[16]	edge coupling	photonic wire bonding	4.2	InP and silicon	@ 1493 nm	Active
This work	Edge coupling with mode size converting	Free-space coupler	2.2	multi-platform	1480 nm-1620 nm	Passive

S2. Requirements in mode size conversion

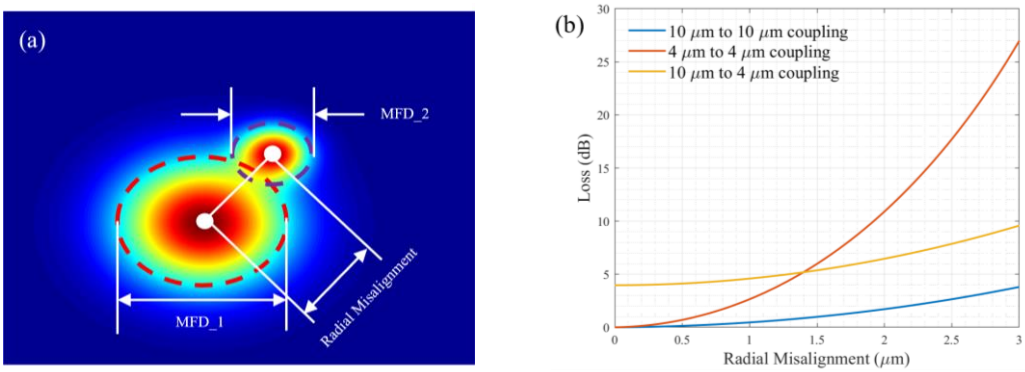

Figure S1. plot of the mode coupling loss introduced by limited printing accuracy at different MFDs. (a) The loss evaluation considering two fundamental modes that are in near-Gaussian equilibrium mode distribution and have a radial misalignment no larger than (MFD_1+MFD_2)/2. (b) Loss to misalignment curve for the cases of 10 μm-to-10 μm (blue solid line), 4 μm-to-4 μm (red solid line), and 10 μm-to-4 μm (yellow solid line) couplings.

Truly passive alignment in optical coupling features a large tolerance. In instances where the Mode Field Diameters (MFDs) of paired modes are large, the aligning window is typically significantly expanded compared with smaller mode sizes. Evaluations are made considering a near-Gaussian equilibrium mode distribution [17]. The coupling efficiency, η, can be calculated as:

$$\eta = \frac{|\int E_1 * E_2 dA|^2}{\int |E_1|^2 dA \int |E_2|^2 dA} \tag{S1}$$

where E_1 and E_2 are the complex electric fields of the modes in the coupling plane, respectively.

The complex electric fields of the modes E_1 and E_2 are plotted in MATLAB. The MFD equals the diameter of the Gaussian beam where the intensity I, drops to the cut-off value of:

$$I = I_0 e^{-2} \tag{S2}$$

where I_0 is the peak intensity. Since the MFD d, is defined as two times of the spot size parameter ω, which is proportional to the full width at half maximum (FWHM), then the MFD can be calculated with:

$$d = 2\omega = \frac{FWHM}{\sqrt{2ln2}} \tag{S3}$$

In Gaussian distribution, the FWHM equals to:

$$FWHM = 2\sqrt{2ln2}\sigma \tag{S4}$$

where σ is the standard deviation. Hence, the MFD is denoted as:

$$d = 2\sigma \tag{S5}$$

Then, an offset is introduced to the centers of the two modes as the misalignment. Applying Eq. S1, we can have the coupling efficiency calculated. In such a way, Fig. 2i and Fig. S1b are plotted. As illustrated in Fig. S1(a), the relationship between MFD and alignment tolerance is elucidated. In Fig. S1(b), for the case of a 10 μm-to-10 μm symmetrical mode coupling, the loss to misalignment curve is plotted as a solid blue line; a 4 μm-to-4 μm coupling case is plotted as a solid red line; and an asymmetrical case of 10 μm-to-4 μm coupling is plotted as a yellow solid

line. From the plot, we know that the 10 μm-to-10 μm case has the largest 1 dB-loss misalignment tolerance. When the fiber/chip MFDs difference is large (ie. 10 μm vs. 4 μm), the 1 dB-loss misalignment tolerance is larger than 1 μm, and the loss mainly comes from the mode mismatch. When the 10 μm mode is converted to have a perfect match with the 4 μm mode, the misalignment becomes the dominating factor (case 4 μm-to-4 μm).

Functioning as the primary optical component in the system, the mode size converter incorporates a pair of parabolic-shaped reflectors. In this design, incident light from an input waveguide is directed into the initial segment of the coupling unit, undergoing two reflections at the polymer/air interfaces. Subsequently, the light is redirected through the second part and into a second waveguide. The parabolic shape is meticulously optimized to precisely manipulate the propagation of light within the reflector. When the two parabolic reflectors are symmetrical, the output MFD remains constant. Introducing variations to the dimensions of the second mode reflector facilitates the alteration of the MFD of the output mode, achieving effective mode size conversion. The inherent free space propagation of light within the coupler, coupled with its 3D design flexibility, allows for arbitrary and broad bandwidth coupling to be seamlessly attained.

S3: Printing recipe development

Two-photon polymerization (2PP) technology, as a forefront in advanced manufacturing, utilizes unique nonlinear absorption of femtosecond laser pulses to precisely fabricate microstructures. Center to this technology is the meticulous recipe tuning, where adjustments in laser intensity, exposure time, and scanning speed determine the resolution, geometry precision, and mechanical properties of fabricated microstructures. More importantly, the printing quality of the parabolic lens, which has a large effect on light transmission efficiency.

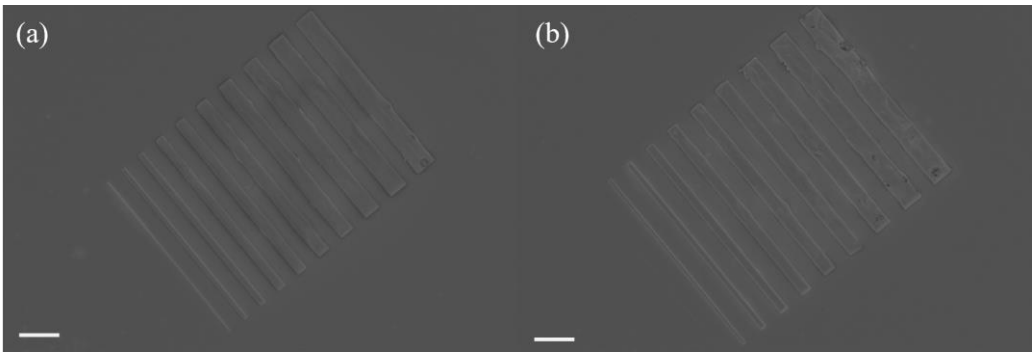

Figure S2. SEM images of polymer waveguides with different printing recipe. (a) waveguides fabricated using optimized recipe (laser power 40 mW, scan speed 100000 μm s^{-1}), (b) waveguides use default recipe (laser power 100 mW, scan speed 100000 μm s^{-1}). All scale bars 20 μm.

In the fabrication process, the laser power and scan speed matter the most. Nanoscribe Photonics Professional GT2 is equipped with a femtosecond fiber laser with a center wavelength of 780 nm. The default laser power and scan speed of the laser are 50 mW and 100000 μm s^{-1}respectively, which provides good enough printing quality for general applications. However, as we are in a situation where any imperfection will lead to additional coupling loss, fine-tuning the printing recipes is critical. To achieve optimum performance, the laser power and scan speed must be carefully examined. In this work, a combination of 40 mW laser power and 100000 μm s^{-1} scan speed is adopted for a balance on printing time and accuracy. When printing on chips, the laser power is reduced by 5-10 mW subject to conditions. Figure S2 are top-view SEM images taken from the dose test sample.

S4: Detailed alignment process of Si and InP chips

The alignment procedure for the Si and InP chips involves an initial mechanical alignment process followed by further refinement using Nanoscribe. Mechanical fixers and clamps are first fabricated in accordance with the chip geometry. The gap between different fixers is set to be 5-10 μm lareger than the chip dimensions to allow sufficient room for chip insertion. Simultaneously, the supporting polymer pad is printed alongside the fixers and clamps in a one-step process using IP-S, ensuring high printing accuracy and alignment. A mechanical coupling frame is developed following Nanoscribe's standard procedure, and subesequently, the chips are inserted. For enhanced adhesion, wax and resins can be employed. While the mechanical coupling frame ensures assembly accuracy, achieving sub-micron alignment between optical interfaces proves still challenging.

Upon completion of the mechanical assembly, the entire structure, comprising chips, fixers, clamps, and polymer pad, is immersed in IP-n162 and sent to Nanoscribe for precise alignment. The built-in interface finder of Nanoscribe can accurately locates the chip-resin interface, facilitating the assessment of height differences between chips. Additionally, Nanoscribe's built-in camera aids in in-plane alignment by making the waveguide visible. Subtle rotations and adjustments of the parabolic-shaped structure enable the attainment of sub-micron-level alignment.

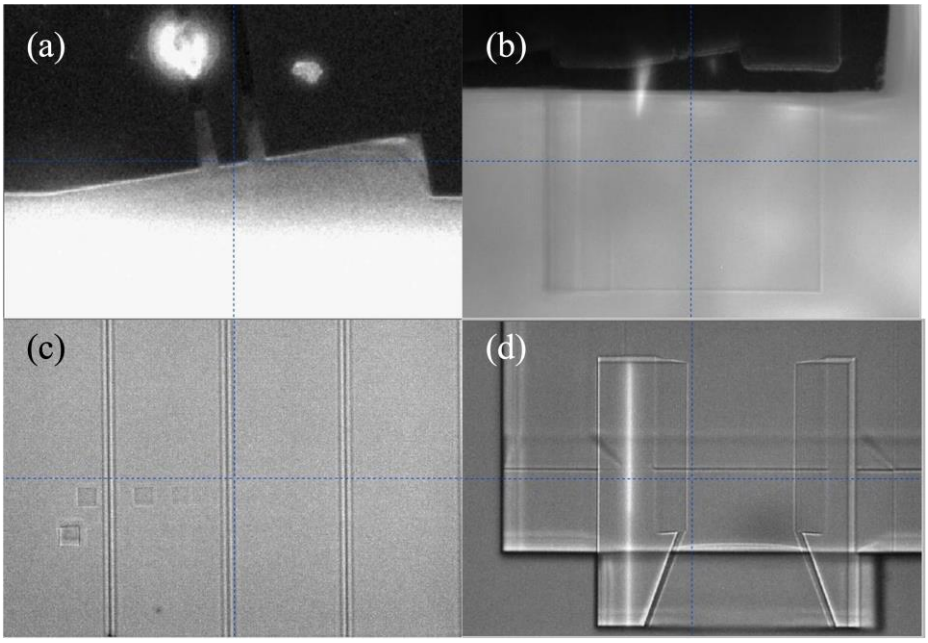

Figure S3. Pictures from built-in camera of Nanoscribe. (a) center cursor helping in-plane alignment of printing, (b) checking object position while printing to ensure good alignment, (c) finding the interface position of the top layer, (d) overlap setting with built-in camera.

S5: Process flow for the fabrication of the full-polymeric test chips

Detailed process flow for a full-polymeric test chip is depicted in the following figure. A block of resin is first printed on the carrier, which can either be a piece of glass or a silicon chip, and will later serve as the substrate of the whole testing structure. We use IP-S for the substrate, which is a photosensitive resin that has a relatively low refractive index provided by Nanoscribe. At the edge of the substrate, we introduce a set of align markers to facilitate the alignment process of the following steps. Then a polymer waveguide is printed using IP-n162, which has a higher refractive index than IP-S, to enable mode confinement. The parabolic-shaped reflectors are then printed at each end of the polymer waveguide, and precise alignment is ensured with the markers. Finally, the funnel-like structures are

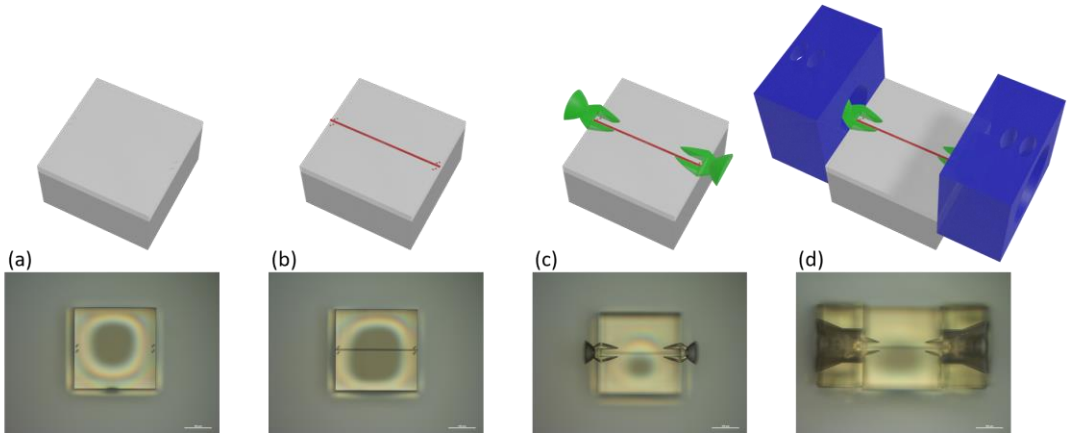

Figure S4. Schematics (upper) and optical microscope images (lower) of the test sample preparation steps. (a) Print a base with IP-S resin which has a refractive index of 1.504 at the wavelength of 950 nm. The base layer helps to prohibit mode leaking during propagation. A pair of align markers are introduced at the edge of the base to enable coordination correction during the printing of the following structures. (b) The polymeric waveguide sits on the base. The photo-sensitive resin for the waveguide printing is IP-n162, which has a refractive index of 1.602 at the wavelength of 950 nm. (c) The parabolic-shaped reflectors are prepared at each end of the waveguide to couple the laser signal in/out of the test chip. The bayonet structure is split to avoid interaction with the waveguide. (d) The mechanical structure is printed over the reflectors to realize the passive alignment for the optical fibers.

printed on the substrate to accommodate optical fibers during the coupling efficiency test. When creating the printing job for the funnels, some overlap with the substrate is needed to enhance the mechanical stability. The test results are presented in the main body of the paper.

References

1. P.-I. Dietrich et al., “Lenses for Low-Loss Chip-to-Fiber and Fiber-to-Fiber Coupling Fabricated by 3D Direct-Write Lithography,” 2016.
2. P. I. Dietrich et al., “In situ 3D nanoprinting of free-form coupling elements for hybrid photonic integration,” Nat Photonics, vol. 12, no. 4, pp. 241–247, Mar. 2018.
3. O. A. J. Gordillo, M. A. Tadayon, Y.-C. Chang, and M. Lipson, “3D photonic structure for plug-and-play fiber to waveguide coupling,” 2018.
4. M. Blaicher et al., “3D-Printed Ultra-Broadband Highly Efficient Out-of-Plane Coupler for Photonic Integrated Circuits,” 2018.
5. H. Gehring, A. Eich, C. Schuck, and W. H. P. Pernice, “Broadband out-of-plane coupling at visible wavelengths,” Opt Lett, vol. 44, no. 20, p. 5089, Oct. 2019.
6. H. Gehring et al., “Low-loss fiber-to-chip couplers with ultrawide optical bandwidth,” APL Photonics, vol. 4, no. 1, Jan. 2019.
7. S. Yu, H. Zuo, X. Sun, J. Liu, T. Gu, and J. Hu, “Optical Free-Form Couplers for High-density Integrated Photonics (OFFCHIP): A Universal Optical Interface,” Journal of Lightwave Technology, vol. 38, no. 13, pp. 3358–3365, Jul. 2020.
8. O. A. Jimenez Gordillo, S. Chaitanya, Y.-C. Chang, U. D. Dave, A. Mohanty, and M. Lipson, “Plug-and-play fiber to waveguide connector,” Opt Express, vol. 27, no. 15, p. 20305, Jul. 2019.
9. H. Luo, F. Xie, Y. Cao, S. Yu, L. Chen, and X. Cai, “Low-loss and broadband fiber-to-chip coupler by 3D fabrication on a silicon photonic platform,” Opt Lett, vol. 45, no. 5, p. 1236, Mar. 2020.
10. A. Cordero-Davila, J. R. Kantun-Montiel, and J. Gonzalez-Garcia, in *Imaging and Applied Optics Technical Digest 2012* (Optical Society of America, 2012), p. 13.
11. Y. Xu et al., “3D-printed facet-attached microlenses for advanced photonic system assembly,” Light: Advanced Manufacturing, vol. 4, no. 1, p. 1, 2023
12. A. Marinins et al., “Wafer-Scale Hybrid Integration of InP DFB Lasers on Si Photonics by Flip-Chip Bonding With sub-300 nm Alignment Precision,” IEEE Journal of Selected Topics in Quantum Electronics, vol. 29, no. 3, May 2023, doi: 10.1109/JSTQE.2022.3223641.
13. X. Zhang et al., “Heterogeneous integration of III-V semiconductor lasers on thin-film lithium niobite platform by wafer bonding,” Appl Phys Lett, vol. 122, no. 8, Feb. 2023, doi: 10.1063/5.0142077.
14. Y. Pan et al., “Heteroepitaxy of semiconducting 2H-MoTe2 thin films on arbitrary surfaces for large-scale heterogeneous integration,” Nature Synthesis, vol. 1, no. 9, pp. 701–708, Sep. 2022, doi: 10.1038/s44160-022-00134-0.
15. B. Haq et al., “Micro-Transfer-Printed III-V-on-Silicon Distributed Feedback Lasers,” in 2020 Optical Fiber Communications Conference and Exhibition, OFC 2020 - Proceedings, Institute of Electrical and Electronics Engineers Inc., Mar. 2020. doi: 10.1364/oe.404847.
16. M. Billah et al., “Multi-Chip Integration of Lasers and Silicon Photonics by Photonic Wire Bonding,” 2015.
17. G. J. Spühler et al., "Experimentally confirmed design guidelines for passively Q-switched microchip lasers using semiconductor saturable absorbers." JOSA B 16.3 (1999): 376-388.